

# Shared-Spectrum Multistatic Radar: Experimental Demonstration using FM Waveforms

Patrick M. McCormick and Shannon D. Blunt  
University of Kansas  
Radar Systems Lab (RSL)  
Lawrence, Kansas, USA

**Abstract**—In light of the rapidly growing interest in spectrum sharing capabilities, we examine the prospect of multiple radars concurrently occupying the same spectrum, where the associated emissions mutually interfere in the form of waveform cross-correlation effects. To assess the practical separability of the resulting radar echoes a new version of the multistatic adaptive pulse compression (MAPC) algorithm is formulated that is applicable to FM waveforms, which remain the most commonly used in operational radar systems. It is demonstrated experimentally that this method provides effective shared-spectrum signal separation, especially when preceded both other forms of coherent gain to maximize the available dynamic range.

**Index Terms**—multistatic radar, spectrum sharing, MIMO, adaptive filtering

## I. INTRODUCTION

Due to steadily increasing demand for spectrum there has been a recent surge in research on spectrum sharing topics, particularly with regard to radar and communication spectrum sharing [1]–[6]. Radar spectrum is especially coveted because the bands tend to be relatively large to enable good range resolution and spectral maneuverability [7]. Further, the driving factor of high sensitivity has previously precluded the influx of other interference-generating spectrum users into radar bands.

In contrast to the contemporaneous notions of sharing radar spectrum with other users, here we consider how radar may more efficiently use its allocated spectrum by leveraging the same concept of spectral re-use employed for commercial communications. Specifically, if a radar receiver has coherent knowledge of the other radar waveforms being employed in its vicinity, how well can the associated echoes be separated via receive processing? Put another way, can we address the problem of RF fratricide that is already known to exist, most notably due to atmospheric ducting effects [8]?

This problem was addressed a little over a decade ago via the Multistatic Adaptive Pulse Compression (MAPC) algorithm [9], [10] that is a multi-waveform generalization of the APC algorithm [11]. However, the previous work on MAPC considered polyphase codes, whose use in practice are limited due to broad spectral skirts (due to abrupt phase transitions) and their subsequent susceptibility to distortion in high-power transmitters [12]. Recent work [13]–[15] has shown how APC can be modified to make it suitable to arbitrary FM waveforms, which are far more suitable to high-power systems. Here we extend this recent work to likewise demonstrate the efficacy of an FM suitable variant of MAPC that may

facilitate the feasibility of shared-spectrum radar. In so doing it is shown that the traditional ordering of operations in the receive processing chain, with Doppler processing following pulse compression, could benefit from a converse arrangement. Further, achievement of the enhanced sensitivity enabled by adaptive processing in the range domain also introduces a heightened need for range-walk compensation to ensure adequate fidelity is maintained. These factors establish a trade-space between complexity and performance that underscore the difficulty with the practical realization of all manner of radar spectrum sharing.

## II. SHARED-SPECTRUM RADAR RECEIVE PROCESSING

Consider the scenario where multiple radar transmitters concurrently emit unique waveforms occupying the same frequency band. When faced with the superposition of scattering by multiple waveforms, conventional range-domain processing (i.e. matched filtering) suffers from a significant amount of interference arising from the cross-correlation between the different waveforms. Here we formulate a variant of the MAPC algorithm [9] to facilitate the adaptive separation of these components within the context of physically realizable waveforms.

Clearly there are complicating issues such as partial spectral overlap, imperfect knowledge of other radar waveforms (and their possibly too-similar nature), transmit/receive timing synchronization (or lack thereof), and the damage that could be caused to sensitive receive components by the direct mainbeam illumination of another high-power radar. These effects notwithstanding, the proposed approach and subsequent experimental performance assessment establish a benchmark for what could be achieved in practice. Further, this formulation may also have application to a variety of downstream MIMO processing that relies on a high degree of waveform separability (theoretically orthogonal) and other structure-based separation of radar and communication signals.

### A. Signal model

Consider  $D$  transmitters that emit unique frequency modulated (FM) waveforms having the same spectral support. For the sake of convenience, assume that the  $D$  emitted waveforms have the same pulsewidth  $T$  and 3-dB bandwidth  $B$ , and are receive sampled at a rate commensurate with sampling period  $T_s$ . Thus the waveforms can be represented as length- $N$

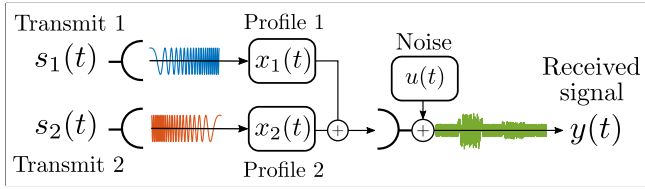


Fig. 1. Two-transmitter multistatic configuration and signal model.

discrete sequences  $\mathbf{s}_i = [s_i(1) \cdots s_i(N)]^T$  for  $i = 1, \dots, D$  and  $N = T/T_s$ . Note that the sampling rate  $f_s = 1/T_s$  must sufficiently exceed  $B$  to ensure enough fidelity for receive separation.

For a receiver that captures the echoes from these  $D$  transmitters the resulting discretized signal at sample delay  $\ell$  can be modeled as the superposition of convolutions

$$y(\ell) = \sum_{i=1}^D \sum_{n=1}^N s_i(n)x_i(\ell - n + 1) + u(\ell), \quad (1)$$

where  $x_i(\ell)$  is the complex scattering amplitude at delay  $\ell$  associated with the  $i$ th transmitter and  $u(\ell)$  is additive noise. A simple two-transmitter multistatic configuration is illustrated in Figure 1.

The collection of  $N$  samples of the received signal corresponding to scattering at delay  $\ell$  can then be expressed as

$$\mathbf{y}(\ell) = [y(\ell) \cdots y(\ell + N - 1)]^T = \sum_{i=1}^D \mathbf{S}_i \mathbf{x}_i(\ell) + \mathbf{u}(\ell). \quad (2)$$

The length  $N$  vector  $\mathbf{u}(\ell)$  constitutes additive noise while the length  $2N - 1$  vector  $\mathbf{x}_i(\ell) = [x_i(\ell - N + 1) \cdots x_i(\ell + N - 1)]^T$  comprises the complex scattering of the  $i$ th range profile surrounding and including delay  $\ell$ . Finally, the Toeplitz matrix

$$\mathbf{S}_i = \begin{bmatrix} s_i(N) & \cdots & \cdots & s_i(1) & 0 & \cdots & 0 \\ 0 & \ddots & & \vdots & \ddots & \ddots & \vdots \\ \vdots & \ddots & \ddots & \vdots & & \ddots & 0 \\ 0 & \cdots & 0 & s_i(N) & \cdots & \cdots & s_i(1) \end{bmatrix} \quad (3)$$

facilitates the convolution of the  $i$ th waveform with  $\mathbf{x}_i(\ell)$ .

The received signal vector  $\mathbf{y}(\ell)$  represents the response from a single pulse emitted from each of the  $D$  transmitters. By extension, the collection of echoes from  $P$  pulses into a coherent processing interval (CPI) yields the pulse-Doppler data matrix

$$\mathbf{Y}(\ell) = [\mathbf{y}_1(\ell) \quad \mathbf{y}_2(\ell) \cdots \mathbf{y}_P(\ell)], \quad (4)$$

where each column has the structure of (2) for a particular pulse.

Standard range-Doppler processing of the model in (4) would involve pulse compression (for each waveform) of the echoes from each pulse followed by Doppler processing across the set of  $P$  pulse responses. These operations are linear, and thus reversible, but this order remains the norm. However, as will be discussed in the next section, the separation of

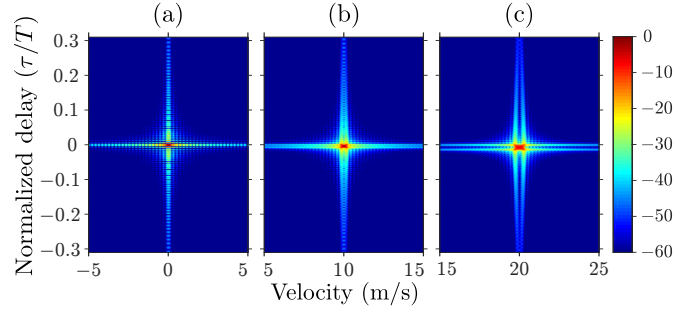


Fig. 2. Effects of range walking on DFT-based range-Doppler processing for scatterers moving at (a) 0 m/s, (b) 10 m/s, and (c) 20 m/s.

echoes produced by shared-spectrum waveforms behaves the swapping of these operations.

### B. Order of operations and range-walk compensation

The separation of the  $D$  echo responses within a given receiver involves the suppression of both the autocorrelation sidelobes for one waveform and the cross-correlation sidelobes arising from the other  $D - 1$  waveforms. Since these sidelobes can only be adaptively suppressed to the level of the noise floor, it is therefore beneficial to maximize the SNR (and thus dynamic range) of the data beforehand through other forms of coherent gain, namely beamforming and Doppler processing. Of course, applying Doppler processing prior to adaptive pulse compression does introduce a fidelity-limiting effect that must also be addressed.

Typically, Doppler processing is performed via discrete Fourier transform (DFT) across the pulses of a range-Doppler data matrix similar to (4), albeit usually with pulse compression having already been performed [16]. That said, if a scatterer traverses multiple range resolution cells during the CPI (i.e. range-walking), the resulting Doppler response of said scatterer will be spread over multiple range cells.

Figure 2 shows the range-Doppler responses produced by matched filter pulse compression and subsequent DFT Doppler processing for three scatterers moving at speeds of 0 m/s, 10 m/s, and 20 m/s. The transmit parameters, which are the same as those used for experimental demonstration in Sect. IV, are 1.5 m range resolution, 200 ms CPI, and 200  $\mu$ s pulse repetition interval (PRI). The three scatterers are therefore moving at range rates of 0, 1.33, and 2.66 range resolution cells per CPI interval. Compared to the stationary scatterer, the scatterers moving at 10 m/s and 20 m/s produce distorted responses due to range walking, thus resulting in correlation peak losses of 2.41 dB and 7.72 dB, respectively.

The effects of range-walking can be compensated by delay-shifting the columns of (4) by the expected sample amount (typically non-integer) associated with a particular velocity  $v$  as

$$\mathbf{Y}(\ell, v) = [\mathbf{y}_1(\ell) \quad \mathbf{y}_2(\ell - f_s \Delta t_v) \cdots \mathbf{y}_P(\ell - f_s(P-1)\Delta t_v)], \quad (5)$$

where

$$\Delta t_v = \frac{2v}{c} \times \text{PRI} \quad (6)$$

is the pulse-to-pulse time shift of a scatterer moving at velocity  $v$ , for  $c$  the speed of light. This process aligns the envelopes of the received pulses for this theoretical scatterer, though it does not align the phases. Thus, the coherent receive data vector for velocity  $v$  can be found via application of a DFT as

$$\mathbf{y}(\ell, v) = \frac{1}{P} \mathbf{Y}(\ell, v) (\mathbf{h} \odot \mathbf{a}(v, \lambda_c)), \quad (7)$$

where  $\mathbf{h}$  is a  $P \times 1$  taper to control Doppler sidelobes (e.g. a Hamming window),  $\odot$  is the Hadamard product, and

$$\mathbf{a}(v, \lambda_c) = \left[ 1 \quad e^{-j \frac{4\pi v}{\lambda_c} \text{PRI}} \quad \dots \quad e^{-j(P-1) \frac{4\pi v}{\lambda_c} \text{PRI}} \right]^T \quad (8)$$

is the  $P \times 1$  DFT vector for velocity  $v$  and carrier wavelength  $\lambda_c$ .

The Doppler processed data at delay  $\ell$  and velocity  $v$  can then be approximated by the model

$$\mathbf{y}(\ell, v) \simeq \sum_{i=1}^D \mathbf{S}_i \tilde{\mathbf{x}}_i(\ell, v) + \mathbf{u}(\ell, v) \quad (9)$$

where  $\tilde{\mathbf{x}}_i(\ell, v) = [\tilde{x}_i(\ell - N + 1, v) \cdots \tilde{x}_i(\ell + N - 1, v)]^T$  is the  $i$ th length  $2N - 1$  range profile vector corresponding to scatterers moving at a velocity  $v$  as well as Doppler sidelobe energy from other scatterers moving at different velocities but the same ranges. The impact of this sidelobe energy can be reduced by using a Doppler taper. The model in (9) is used in the MAPC formulation derived in the next section to generate range and velocity dependent filters that estimate the compensated response  $\tilde{x}_i(\ell, v)$ . This form is particularly important here because the achievement of good separation dictates the need for high fidelity.

### III. MULTISTATIC ADAPTIVE PULSE COMPRESSION

The derivation of the MAPC filters is based on a gain-constrained MMSE framework, where it is assumed that the discretized transmit waveforms  $\mathbf{s}_i$  for  $i = 1, \dots, D$  are known at the receiver. It has been found that model mismatch due to straddling and unintentional super-resolution caused by over-sampling (necessary for high fidelity) can degrade performance of the APC formulation in practice. However, recent modifications have demonstrated how these effects can be addressed for practical waveforms, particularly FM [13]–[15]. Here we shall apply these same modifications to the MAPC algorithm within this range-walk compensated context.

#### A. Derivation of MAPC filters

The MAPC filter  $\mathbf{w}_i(\ell)$  that facilitates estimation of  $\tilde{x}_i(\ell, v)$  is obtained by solving the gain-constrained MMSE problem [17]

$$\begin{aligned} \underset{\mathbf{w}_i^*(\ell, v)}{\text{minimize}} \quad & E \left[ |\tilde{x}_i(\ell, v) - \mathbf{w}_i^H(\ell, v) \mathbf{y}(\ell, v)|^2 \right] \\ \text{subject to} \quad & \mathbf{w}_i^H(\ell, v) \mathbf{s}_i = 1 \end{aligned} \quad (10)$$

where  $E[\bullet]$  is the expected value. The closed-form solution of (10) results in the MVDR-like form

$$\mathbf{w}_i(\ell, v) = \frac{\mathbf{R}^{-1}(\ell, v) \mathbf{b}_i(\ell, v)}{\mathbf{s}_i^H \mathbf{R}^{-1}(\ell, v) \mathbf{b}_i(\ell, v)} \quad (11)$$

where

$$\mathbf{b}_i(\ell, v) = E[\mathbf{y}(\ell, v) \tilde{x}_i^*(\ell, v)] \quad (12)$$

and

$$\mathbf{R}(\ell, v) = E[\mathbf{y}(\ell, v) \mathbf{y}^H(\ell, v)]. \quad (13)$$

Here, we assume that the range profiles  $\tilde{x}_i(\ell, v)$  are uncorrelated such that

$$E[\tilde{x}_i(\ell, v) \tilde{x}_j^*(\bar{\ell}, v)] = \begin{cases} E[|\tilde{x}_i(\ell, v)|^2] & \text{for } \ell = \bar{\ell}, i = j \\ 0 & \text{otherwise} \end{cases} \quad (14)$$

and that the noise is white Gaussian with zero mean and variance  $\sigma^2$ . Therefore, using the compensated model of  $\mathbf{y}(\ell, v)$  from (9), the expectations in (12) and (13) become

$$\mathbf{b}_i(\ell, v) = E[|\tilde{x}_i(\ell, v)|^2] \mathbf{s}_i \triangleq |\hat{x}_i(\ell, v)|^2 \mathbf{s}_i \quad (15)$$

and

$$\begin{aligned} \mathbf{R}(\ell, v) &= \sum_{j=1}^D \mathbf{S}_j E[\tilde{\mathbf{x}}_j(\ell, v) \tilde{\mathbf{x}}_j^H(\ell, v)] \mathbf{S}_j^H + E[\mathbf{u}(\ell, v) \mathbf{u}^H(\ell, v)] \\ &\triangleq \sum_{j=1}^D \mathbf{S}_j \mathbf{P}_j(\ell, v) \mathbf{S}_j^H + \sigma^2 \mathbf{I}_N \end{aligned} \quad (16)$$

for  $\hat{x}_i(\ell, v)$  the current estimate of  $\tilde{x}_i(\ell, v)$ . Further,  $\mathbf{I}_N$  is the  $N \times N$  identity matrix and

$$\mathbf{P}_i(\ell, v) = (\hat{\mathbf{x}}_i(\ell, v) \hat{\mathbf{x}}_i^H(\ell, v)) \odot \mathbf{I}_{2N-1} \quad (17)$$

is a diagonal matrix containing the squared-magnitude of the current estimates  $\hat{\mathbf{x}}_i(\ell, v) = [\hat{x}_i(\ell - N + 1, v) \cdots \hat{x}_i(\ell + N - 1, v)]^T$ .

The reiterative structure of MAPC arises from the approximation of  $E[|\tilde{x}_i(\ell, v)|^2]$  by the current estimate  $|\hat{x}_i(\ell, v)|^2$ , which is initialized by the  $D$  matched filter responses. Each successive iteration then uses the most recent estimate of these responses, which were updated in the previous iteration. It has been found that 1-4 iterations are typically needed to converge to a good estimate of the scattering profiles.

#### B. Modifications to MAPC for FM waveforms

To facilitate the application of MAPC for FM waveforms two modifications to the structured covariance matrix of (16) are needed [13]. The first prevents mainlobe super-resolution arising from over-sampling, that would otherwise significantly hinder sidelobe suppression [18]. The second addresses the model mismatch caused by range straddling effects [19].

The peak-to-null mainlobe width of an FM waveform is  $K$  samples, where  $K = f_s/B$  is the receiver over-sampling factor for waveform 3-dB bandwidth  $B$  (for simplicity we consider  $K$  to be an integer). Therefore, the super-resolution condition can be avoided by zeroing out the  $\{N - K + 1, \dots, N - 1\}$  and  $\{N + 1, \dots, N + K - 1\}$  columns of  $\mathbf{S}_i$ , which are highly correlated with the  $N$ th column due to over-sampling. Alternatively, one could modify the matrix from (17) as

$$\tilde{\mathbf{P}}_i(\ell, v) = (\hat{\mathbf{x}}_i(\ell, v) \hat{\mathbf{x}}_i^H(\ell, v)) \odot \bar{\mathbf{I}}_{2N-1, K} \quad (18)$$

where  $\bar{\mathbf{I}}_{2N-1, N}$  is an identity matrix with the  $\{N - K + 1, \dots, N - 1\}$  and  $\{N + 1, \dots, N + K - 1\}$  elements of the main diagonal set to zero.



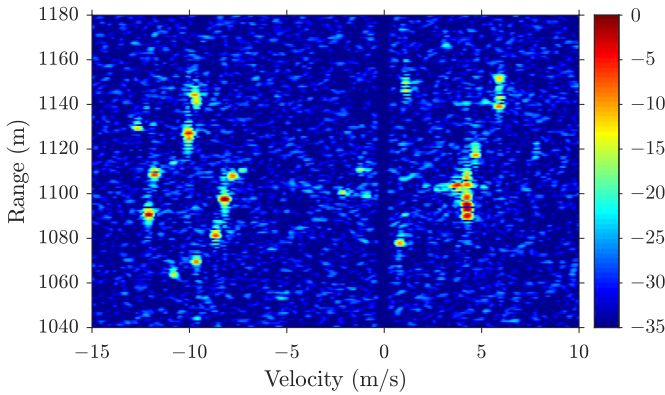


Fig. 5. RD response for down-chirp LFM only (Case 1).

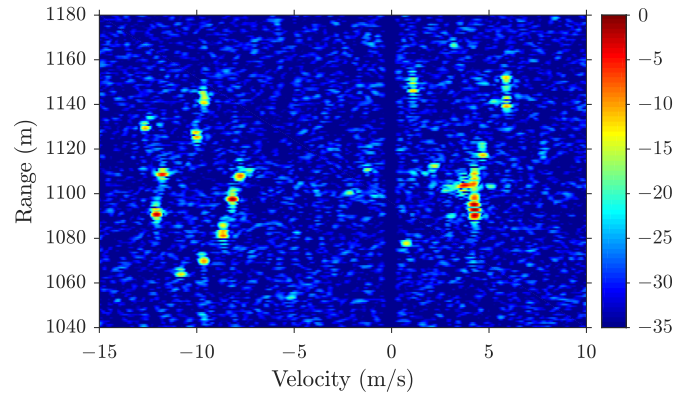


Fig. 6. RD response for up-chirp LFM only (Case 2).

The Doppler processed response for Case 3 was subsequently processed using both matched filtering (22) and MAPC (21) with 3 iterations. To illustrate the benefit of Doppler processing gain prior to MAPC, an additional scenario is included whereby MAPC is first performed on each presumed pulse followed by Doppler processing.

Figures 5 and 6 show the range-Doppler (RD) responses for Cases 1 and 2 after range-walk compensated Doppler processing and matched filter pulse compression. Because the two transmitters are located close to one another the two cases produce very similar responses that include many high SNR moving targets.

Figures 7 and 8 show the range-Doppler responses for the shared-spectrum emission in Case 3 using matched filtering (with down-chirp and up-chirp, respectively) after Doppler processing. In both figures the additional signal results in significant interference due to the cross-correlation between the two waveforms, which is indicated by the vertical striations that look like extended range sidelobes. Note that if these radars were not collocated or if they illuminated different spatial regions, these cross-correlation effects could appear anywhere within the scene of interest.

Now compare the Case 3 matched filter results from Figs. 7 and 8 with the MAPC processed results in Figs. 9 and 10 (for Tx 1 and Tx 2, respectively). Note how the cross-correlation interference has now been suppressed. In fact, comparing the shared-spectrum MAPC responses with the previous single-waveform matched filter results in Figs. 5 and 6, it is observed that MAPC has also suppressed the LFM range sidelobe response.

Finally, it is worth examining the benefit provided by performing Doppler processing prior to MAPC. Figures 11 and 12 again illustrate the MAPC responses for Tx 1 and Tx 2, respectively, albeit now with the Doppler processing occurring after the adaptive pulse compression. It is observed that MAPC is only able to suppress sidelobes to the level of the noise floor (before the additional DFT gain). As such, performing Doppler processing after MAPC coherently integrates the residual cross-correlation effects that were below the noise floor.

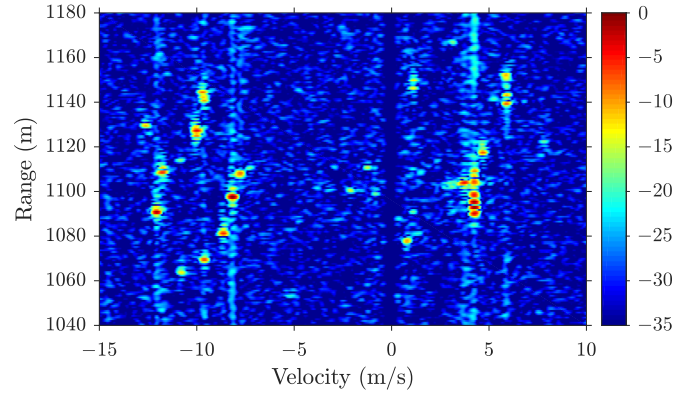


Fig. 7. RD response for shared-spectrum (Case 3) using down-chirp MF.

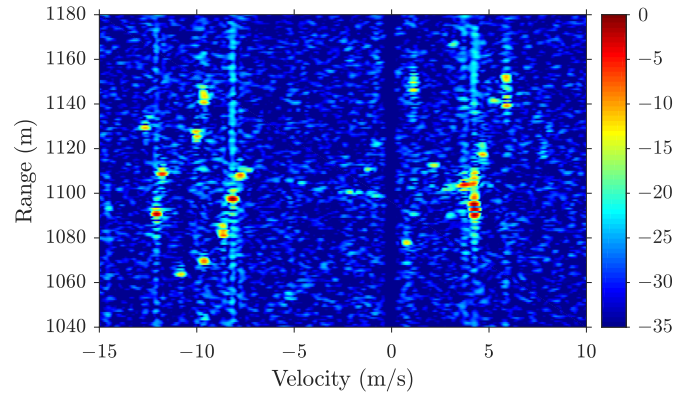


Fig. 8. RD response for shared-spectrum (Case 3) using up-chirp MF.

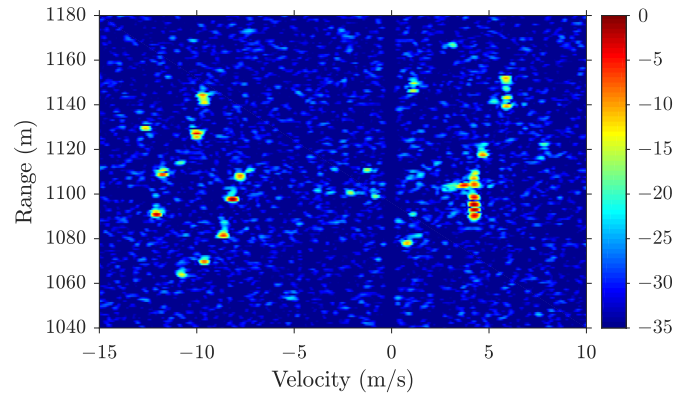


Fig. 9. RD response for shared-spectrum (Case 3) using MAPC, Tx 1.

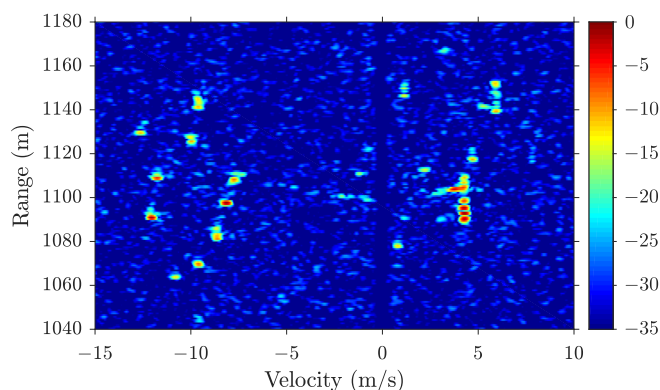


Fig. 10. RD response for shared-spectrum (Case 3) using MAPC, Tx 2.

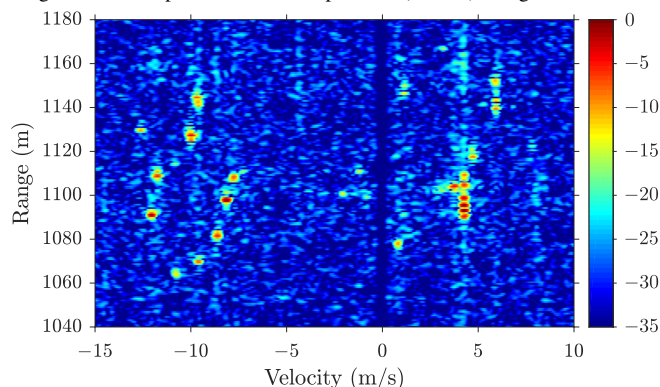


Fig. 11. RD response for Case 3 using MAPC, Tx 1 (MAPC first).

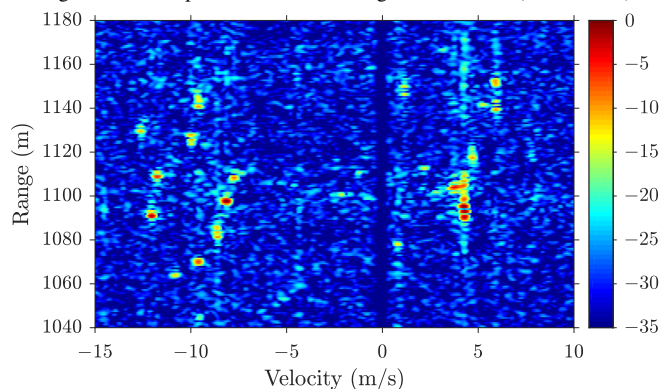


Fig. 12. RD response for Case 3 using MAPC, Tx 2 (MAPC first).

## V. CONCLUSION

A new form of multistatic adaptive pulse compression (MAPC) has been derived for use with FM waveforms in a shared-spectrum radar arrangement. Using LFM waveforms it was then experimentally demonstrated that this practical form of MAPC can separate these shared spectrum echoes to the limit of the noise floor. As such, it is beneficial to perform other coherent processing before MAPC so that the associated gain can maximize the available dynamic range for auto/cross-correlation sidelobe suppression. In addition to illustrating the potentially achievable capabilities of radar-to-radar spectrum sharing (many other practical issues notwithstanding), this formulation could facilitate the actual separation of MIMO emissions that are theoretically treated as orthogonal and also sets the stage for other structure-based interference cancellation between radar and communication systems [23].

## REFERENCES

- [1] S.M. Mishra, A. Sahai, and R.W. Brodersen, "Cooperative sensing among cognitive radios," *IEEE Intl. Conf. on Communications*, vol. 4, Jun. 2006.
- [2] J.M. Peha, "Approaches to spectrum sharing," *IEEE Commun. Mag.*, vol. 43, no. 2, pp. 10–12, Feb. 2005.
- [3] H. Deng and B. Himed, "Interference mitigation processing for spectrum-sharing between radar and wireless communications systems," *IEEE Trans. Aerosp. Electron. Syst.*, vol. 49, no. 3, pp. 1911–1919, Jul. 2013.
- [4] F. Hessar and S. Roy, "Spectrum sharing between a surveillance radar and secondary Wi-Fi networks," *IEEE Trans. Aerosp. Electron. Syst.*, vol. 52, no. 3, pp. 1434–1448, Jun. 2016.
- [5] Z. Khan, J.J. Lehtomaki, R. Vuoltoniemi, E. Hossain, and L.A. Dasilva, "On opportunistic spectrum access in radar bands: lessons learned from measurement of weather radar signals," *IEEE Wireless Commun. Mag.*, vol. 23, no. 3, pp. 40–48, Jun. 2016.
- [6] S.D. Blunt and E.S. Perrins, eds., *Radar & Communication Spectrum Sharing*. IET, 2018.
- [7] H. Griffiths, L. Cohen, S. Watts, E. Mokole, C. Baker, M. Wicks, and S. Blunt, "Radar spectrum engineering and management: technical and regulatory issues," *Proc. IEEE*, vol. 103, no. 1, pp. 85–102, Jan. 2015.
- [8] H.V. Hitney, J.H. Richter, R.A. Pappert, K.D. Anderson, and G.B. Baumgartner, "Tropospheric radio propagation assessment," *Proc. IEEE*, vol. 73, no. 2, pp. 265–283, Feb. 1985.
- [9] S.D. Blunt and K. Gerlach, "Multistatic adaptive pulse compression," *IEEE Trans. Aerosp. Electron. Syst.*, vol. 42, no. 3, pp. 891–903, Jul. 2006.
- [10] S.D. Blunt, T. Higgins, A. Shackelford, and K. Gerlach, "Multistatic & waveform-diverse radar pulse compression," in *Waveform design and diversity for advanced radar systems*, F. Gini, A. De Maio, and L. Patton, eds. IET, 2012, pp. 207–230.
- [11] S.D. Blunt and K. Gerlach, "Adaptive pulse compression via MMSE estimation," *IEEE Transactions on Aerospace and Electronic Systems*, vol. 42, no. 2, pp. 572–584, Apr. 2006.
- [12] S.D. Blunt, M. Cook, J. Jakobosky, J. de Graaf, and E. Perrins, "Polyphase-coded FM (PCFM) radar waveforms, part I: implementation," *IEEE Trans. Aerosp. Electron. Syst.*, vol. 50, no. 3, pp. 2218–2229, Jul. 2014.
- [13] D. Henke, P. McCormick, S.D. Blunt, and T. Higgins, "Practical aspects of optimal mismatch filtering and adaptive pulse compression for FM waveforms," *IEEE Radar Conf.*, May 2015.
- [14] P. McCormick, J. Jakobosky, S.D. Blunt, C. Allen, and B. Himed, "Joint polarization/waveform design and adaptive receive processing," *IEEE Radar Conf.*, May 2015.
- [15] P.M. McCormick, S.D. Blunt, and T. Higgins, "A gradient descent implementation of adaptive pulse compression," *IEEE Radar Conf.*, May 2016.
- [16] M.A. Richards, J. Scheer, W.A. Holm *et al.*, *Principles of modern radar: basic principles*. SciTech Pub., 2010.
- [17] T. Higgins, S.D. Blunt, and K. Gerlach, "Gain-constrained adaptive pulse compression via an MVDR framework," *IEEE Radar Conf.*, May 2009.
- [18] S.D. Blunt, K. Gerlach, and T. Higgins, "Aspects of radar range super-resolution," *2007 IEEE Radar Conf.*, Apr. 2007.
- [19] A.M. Klein and M.T. Fujita, "Detection performance of hard-limited phase-coded signals," *IEEE Trans. Aerosp. Electron. Syst.*, vol. 15, no. 6, pp. 795–802, Nov. 1979.
- [20] S.D. Blunt and T. Higgins, "Dimensionality reduction techniques for efficient adaptive pulse compression," *IEEE Trans. Aerosp. Electron. Syst.*, vol. 46, no. 1, pp. 349–362, Jan. 2010.
- [21] J.R. Guerci, "Theory and application of covariance matrix tapers for robust adaptive beamforming," *IEEE Trans. Signal Process.*, vol. 47, no. 4, pp. 977–985, Apr. 1999.
- [22] T. Cuprak and K.E. Wage, "Efficient Doppler compensated reiterative minimum mean squared error processing," *IEEE Trans. Aerosp. Electron. Syst.*, vol. 53, no. 2, pp. 562–574, Apr. 2017.
- [23] H. Griffiths, S. Blunt, L. Cohen, and L. Savy, "Challenge problems in spectrum engineering and waveform diversity," *IEEE Radar Conf.*, Apr. 2013.